The Astrophysical Journal, 649:1100–1109, 2006 October 1

A STATISTICAL STUDY OF MAIN AND RESIDUAL ACCELERATIONS OF CORONAL MASS EJECTIONS

J. Zhang[1] and K. P. Dere[1]
Received 2006 March 28; accepted 2006 June 10

ABSTRACT

In this paper we present the results of a statistical study of the accelerations of coronal mass ejections (CMEs). A CME usually undergoes a multiphased kinematic evolution, with a main acceleration phase characterized by a rapid increase of CME velocity in the inner corona, followed by a relatively smooth propagation phase characterized by a constant speed or a small residual acceleration in the outer corona. We study both the main acceleration and the residual acceleration for 50 CME events based on Large Angle Spectrometric Coronagraph (LASCO) observations. We find that the magnitude of the main acceleration has a wide distribution, from 2.8 to 4464.0 m s^{-2}, with a median (average) value of 170.1 (330.9 m s^{-2}), and a standard deviation of 644.8 m s^{-2}, whereas the magnitude of the residual acceleration ranges only from -131.0 to 52.0 m s^{-2}, with a median (average) value of 3.1 (0.9 m s^{-2}) and a standard deviation of 25.3 m s^{-2}. The duration of the main acceleration is also widely distributed, from 6 to 1200 minutes, with a median (average) value of 54 (180 minutes) and a standard deviation of 286 minutes.We find an intriguing scaling law between the acceleration magnitude (A) and the acceleration duration (T) over the entire parameter range of almost 3 orders of magnitude, which can be expressed as A (m s^{-2}) $= 10,000T^{-1}$ (minutes). The implications of these observational results on the issues of CME classification and CME modelings are discussed.

Subject headings: Sun: corona — Sun: coronal mass ejections (CMEs)

1. INTRODUCTION

Coronal mass ejections (CMEs) are a large-scale eruptive phenomenon that originate close to the Sun's surface and are accelerated in the Sun's inner corona. They propagate outward into the interplanetary space at a high speed and have a profound impact on the space environment throughout the heliosphere, including the geospace near the Earth. Since the first direct detection of CMEs in the early 1970s, more than 10,000 CMEs have been observed by various coronagraphs, both spaceborne and ground-based. In this paper we present a statistical study on the kinematic properties of CMEs, with a focus on CME's acceleration in the inner corona, which is relatively poorly known compared with the propagation properties of CMEs in the outer corona.

The kinematic properties of CMEs in the outer corona (e.g., $> 2.0\ R_\odot$) are well known from the observations of three major space-based white-light coronagraphs: Solwind (Howard et al. 1985), *Solar Maximum Mission* (*SMM*; Hundhausen et al. 1994), and *Solar and Heliospheric Observatory* (*SOHO*) LASCO (St. Cyr et al. 2000; Yashiro et al. 2004). It has been shown that the distribution of CME velocity in the outer corona ranges from about 50 to 3000 km s^{-1}, with a single peak at about 300 km s^{-1}. The median velocity in the distribution is about 350 km s^{-1}, and the average velocity is about 400 km s^{-1}. On the other hand, an individual CME usually exhibits a more or less constant speed in the outer corona. The distribution of the acceleration in the outer corona is always centered around the value of zero, with a narrow variation within about ± 30 m s^{-2} (Yashiro et al. 2004).

The relatively constant speed of CMEs in the outer corona indicates that CME acceleration takes place mainly in the inner corona, where strong but unstable magnetic field give rise to the eruption. Our earlier study based on several well-observed CME events showed that a CME's full kinematic evolution may undergo three distinct phases: (1) an "initiation phase" of slow rise, (2) an "acceleration phase" of rapid velocity increase, and (3) finally a "propagation phase" with minor velocity variation (Zhang et al. 2001, 2004). The first two phases occur mainly in the inner corona (e.g., $< 2.0\ R_\odot$ or higher), while the third phase is largely in the outer corona (e.g., $> 2.0\ R_\odot$). CME acceleration measured during the acceleration phase in the inner corona is much different from that measured during the propagation phase in the outer corona. For the sake of clarity, we refer the former as main acceleration and the latter as residual acceleration hereafter. The same nomenclature has been used by Chen & Krall (2003) in their theoretical modeling work on CME accelerations.

Observational studies have shown that the CME main acceleration in the inner corona manifests a great diversity, ranging from extremely impulsive evolution to extremely gradual evolution. Events with very strong acceleration (e.g., >1000 m s^{-2}) have been reported (Zhang et al. 2001; Alexander et al. 2002; Gallagher et al. 2003). On the other hand, there is a class of gradual CMEs characterized by very weak (e.g., < 20 m s^{-2}) but persistent long-duration acceleration (e.g., lasting several hours) throughout both the inner and outer corona (Sheeley 1999; Sheeley et al. 1999; Srivastava et al. 1999, 2000). Recently, Zhang et al. (2004) reported a set of three CME events that showed impulsive, gradual, and intermediate acceleration. Most CME events reside between the extremely impulsive ones and the extremely gradual ones, characterized by acceleration on the order of hundreds of m s^{-2}, as seen in many events (Wood et al. 1999; Yurchyshyn 2002; Shanmugaraju et al. 2003; Qiu et al. 2004; Vršnak et al. 2004; Kundu et al. 2004; Sterling & Moore 2005; Jing et al. 2005); note that erupting filaments are used as proxy to track the early acceleration of CME in some studies. St. Cyr et al. (1999) made a statistical study on CME acceleration using 46 CME features observed by ground-based Mauna Loa *K*-coronameter in the inner corona and with the *SMM* coronagraph in the outer corona. They found that the distribution of the acceleration ranged from -218 to 3270 m s^{-2}, with a median (average) value of 44 m s^{-2}

[1] School of Computational Sciences, George Mason University, 4400 University Drive, MSN 5C3, Fairfax, VA 22030.

(264 m s^{-2}). The appearance of negative numbers in the acceleration is due to the fact that they used second-order polynomial fitting to obtain the average acceleration over the entire height range observed; they did not distinguish the main acceleration from the residual acceleration in the fitting.

In this paper we present a statistical study of both the main and the residua accelerations of CMEs based on 50 events well observed by the three overlapping coronagraphs of *SOHO* LASCO. A preliminary and short result based on a small number of events has been reported earlier (Zhang 2005). The observations and event selection is presented in § 2. In § 3 we present two methods to calculate the main acceleration of CMEs: a direct method and an indirect flare-proxy method. A justification of the indirect method and discussion on CME-flare temporal relationship are included in § 3. The results on statistical distributions of CME main accelerations (including both magnitude and duration) and residual accelerations, along with an intriguing finding of an acceleration scaling law, are given in § 4. Discussions on the issues of CME classification and the implications on CME modelings are given in § 5. Conclusions are presented in § 6.

2. OBSERVATIONS AND DATA

The three LASCO coronagraphs, C1, C2, and C3, have complementary fields of view of 1.1–3.0, 2–6, and 4–30 $R_{\odot}$, respectively (Brueckner et al. 1995). For a period of two and a half years (from the launch of *SOHO* in 1995 December to 1998 June), all three coronagraphs operated properly and provided full observations. Unfortunately, C1 failed after the half-year-long malfunction of the *SOHO* spacecraft during 1998. Therefore, this statistical study is limited to the early observations of LASCO, because C1 must be used to reveal CME acceleration in the inner corona. The simultaneous C2 and C3 observations showed CME evolution in the outer corona.

As in almost all CME studies, we use the leading edge (LE), the most outstanding and tractable feature of CME, to identify and measure CME heights in C1. The height-time measurements are subsequently used to calculate CME velocity and acceleration. The use of the LE in CME tracking is appropriate in this study, because it ensures a uniform tracking of the same feature when a CME travels across the C1, C2, and C3 fields of view. While C2 and C3 are typical broadband white-light coronagraphs that observe Thomson-scattered photospheric light scattered by electrons in the corona (the K corona), C1, on the other hand, is a spectroscopic coronagraph that observes the narrow emission lines from highly ionized ions in the corona (the E corona) as well as the K corona. The spectroscopic imaging capability of C1 is achieved by using a Fabry-Perot interferometer that acts as a narrow-passband and tunable filter (passband of about 0.7 Å). C1 operated mainly in the following two strong coronal lines: the green line of Fe XIV at 5302 Å (peak ionization temperature at ~2.0 MK) and the red line of Fe X at 6376 Å (peak ionization temperature at ~1.0 MK). The C1 observing mode was to cyclically take images through multiple points across the profile of one spectral line, and alternate for the two main lines. Because the strength of spectral lines depends on the ionization state of emitting elements, C1 is sensitive to both temperature and density, whereas C2 and C3 are only sensitive to column density of electrons. As a result, the volume feature of CME seen in C1 often appeared much different from that of C2/C3, which makes it difficult to track the internal features of CME across instruments. However, the LE of CME will be unambiguously identified in all three coronagraphs, because of its unique semicircular shape with enhanced brightness in the forefront and enveloping all other trailing features. To facilitate the search, we have made heterogeneous running difference movies, which incorporate all C1 images taken in all wavelengths. By doing this, we are able to greatly enhance the search efficiency and maximize the search results.

C1 observations have a varying cadence depending on wavelength. For instance, on 1997 November 6, a typical 24 hr observing day, C1 took 132 images in total, including 64 images at 5302.4 Å (*green line center*), 15 images at 5302.7 Å, 24 images at 5309.2 Å, 24 images at 6376.4 Å (*red line center*), and five images at 6380.9 Å. Taking into account the images in all wavelengths, C1 had a cadence as short as 2 minutes to as long as 30 minutes. For any single wavelength, the cadence was 20 minutes at best. On the other hand, C2 and C3 had largely regular cadences, which were about 30 and 60 minutes, respectively; the cadences have been about twice as fast after the *SOHO* interruption in 1998.

By searching the C1 image database of about 100,000 images in total, we found 74 CMEs seen in C1, and 50 of them are suitable to be used in this acceleration study. A C1 CME is found if the following two criteria are satisfied: (1) a CME LE, seen as a large-scale semicircular shape of enhanced brightness, clearly showed up in at least one C1 image, and (2) a CME appeared later in the C2 field of view in a consistent position angle and at a consistent time indicating that the eruptive feature seen in C1 was indeed propagating into the C2 field of view. We also found a large number of active features in C1 images; these features include large-scale dimmings and brightenings (often associated with fast CMEs), cavity lifting (often associated with slow CMEs), and loop arcades (posteruption features). However, most of these active events were not selected as C1 CMEs in this study, because their LEs, even present, were not clearly detected. We have documented all C1 activities and the 74 C1 CMEs in our C1 catalog.[2] We excluded 24 C1 CMEs from this study, mainly because we are not able to determine the duration of the main acceleration phase, e.g., only having 1 point of height-time measurement in the acceleration phase.

During the same C1 observing period, LASCO C2 and C3 observed 1112 CMEs in total, listed in the CDAW (Coordinated Data Analysis Workshop) CME catalog generated and maintained by NASA and The Catholic University of America in cooperation with the Naval Research Laboratory.[3] The much smaller number of CMEs seen in C1 is mainly due to the fact that the background induced by the stray light is much higher in C1 because of its approximation to the dominant photosphere. The low signal-to-noise ratio in C1 images prevented most CMEs to be seen. In fact, most CMEs seen in C1 originated close to solar limb. The surface source regions were identified based on eruptive features, including large-scale dimmings and compact brightenings, seen by the Extreme-Ultraviolet Imaging Telescope (EIT, also on board *SOHO*; Delaboudinière et al. 1995). Among the 50 events, 26 originated very close to the limb: all parts of the eruptive features seen in EIT were above the limb. And 19 events were from the front side, but close to the limb. The remaining five events originated from the backside of the Sun: eruptive features were seen in the EIT images neither on the disk nor above the limb. Compared to CMEs that originate close to the limb, a CME from the disk center is more difficult to detect in a coronagraph probably due to the following two effects. The first is the dilution effect: the disk-center CME has already traveled a certain distance, expanded, and hence weakened in brightness when

[2] See http://solar.scs.gmu.edu/research/cme_c1/inde.html.

[3] Available online at http://cdaw.gsfc.nasa.gov/CME_list; please refer to Yashiro et al. 2004 paper for a detailed description of the catalog.

TABLE 1

PROPERTIES OF THE 50 CME EVENTS STUDIED

ID	DATE	TIME (UT) C1	TIME (UT) C2	C1/C2/C3[a]	SOURCE[b] (deg)	FLARE[c]	ONSET (UT)	PEAK (UT)	P.A.[d] (deg)	AW[e] (deg)	VELOCITY (km s^{-1}) Propogaation[f]	VELOCITY (km s^{-1}) Final[g]	ACCELERATION DURATION[h] (minutes)	TY[i]	ACCELERATION (m s^{-2}) Main[j]	ACCELERATION (m s^{-2}) Residual[k]
1.....	1996 Jun 17	02:03	02:23	2/3/3	P080	NA	NA	NA	85	55	304.0	304.0	20	DI	253.3	-3.9
2.....	1996 Jun 19	11:39	11:59	1/4/0	N05E85	B0.9	11:04	11:38	90	57	214.0	214.0	34	FL	104.9	-12.8
3.....	1996 Jul 1	12:46	13:50	1/1/2	P270	B4.0	12:31	12:39	271	52	358.5	358.5	8	FL	746.9	35.3
4.....	1996 Oct 5	08:15	09:37	3/3/7	P250	A2.0	09:00	14:00	266	161	569.0	600.0	300	DU	33.3	16.8
5.....	1996 Oct 19	16:32	17:17	1/3/5	S20E45	B0.6	16:25	17:38	159	170	479.0	479.0	73	FL	109.4	9.4
6.....	1996 Dec 23	11:13	13:28	1/0/11	N05W85	B1.5	10:43	10:53	284	68	263.0	262.4	10	FL	437.4	12.8
7.....	1996 Dec 23	21:04	21:37	2/4/5	S15W75	B4.0	19:50	20:35	255	58	353.7	353.7	33	DI	178.6	4.6
8.....	1996 Dec 24	13:20	13:28	2/4/4	P270	C2.1	13:03	13:11	265	69	324.4	324.4	8	FL	675.7	-1.1
9.....	1996 Dec 27	07:15	08:44	4/9/8	NA	NA	NA	NA	270	63	269.0	269.0	480	DI	9.3	6.8
10.....	1997 Feb 23	00:15	02:55	4/2/4	N25E80	B7.2	02:21	03:33	89	63	903.3	903.3	72	DU	209.1	-4.3
11.....	1997 Apr 4	05:51	06:57	4/12/14	N40E80	NA	NA	NA	280	72	185.0	300.0	900	DI	5.6	3.1
12.....	1997 Apr 9	11:55	12:06	1/3/6	P225	C1.5	10:00	11:40	277	63	484.3	484.3	50	DI	161.4	3.2
13.....	1997 Apr 30	03:41	04:50	4/4/7	P080	A6.0	04:10	05:40	84	71	285.8	285.8	75	DU	63.5	0.4
14.....	1997 May 18	09:01	23:13	8/3/5	NA	NA	NA	NA	88	32	352.9	510.0	700	DI	12.1	17.5
15.....	1997 May 25	14:15	14:48	2/1/4	S28E50	B6.5	14:25	15:00	93	82	683.4	683.4	35	FL	325.4	-2.4
16.....	1997 May 27	09:35	10:15	1/3/6	N02W80	C4.6	09:31	09:57	271	47	428.1	428.1	26	FL	274.5	1.6
17.....	1997 Jun 30	00:04	00:30	3/2/6	N17W82	C1.1	23:41	23:52	275	54	345.2	345.2	11	FL	523.0	-0.4
18.....	1997 Jul 8	14:13	16:09	3/3/0	NA	NA	NA	NA	279	54	75.3	100.0	480	DI	3.5	9.9
19.....	1997 Jul 28	16:09	16:41	4/7/5	P135	NA	NA	NA	99	77	167.4	220.0	40	DI	91.7	-10.8
20.....	1997 Sep 9	19:50	20:06	3/2/5	P315	NA	NA	NA	284	101	726.0	800.0	30	DI	444.4	-7.4
21.....	1997 Sep 16	02:38	04:20	5/5/5	P078	NA	NA	NA	78	72	251.4	350.0	360	DI	16.2	2.6
22.....	1997 Sep 20	09:05	10:20	8/3/7	P250	C2.3	09:49	10:44	272	97	775.9	775.9	55	DU	235.1	5.0
23.....	1997 Sep 28	08:03	08:40	7/4/12	P060	NA	NA	NA	84	60	528.4	528.4	21	DI	419.4	5.5
24.....	1997 Sep 29	14:34	15:46	3/3/7	P045	NA	NA	NA	75	55	699.0	697.8	50	DI	232.6	11.6
25.....	1997 Oct 6	10:13	10:31	3/2/10	P225	NA	NA	NA	273	103	506.0	511.4	20	DI	426.1	3.6
26.....	1997 Oct 12	05:59	06:26	2/2/5	P225	B2.3	06:02	06:54	258	62	777.6	777.6	52	FL	249.2	-3.1
27.....	1997 Oct 18	05:11	06:40	2/3/0	P120	NA	NA	NA	96	50	234.5	380.0	180	DI	35.2	14.6
28.....	1997 Oct 19	02:37	08:06	10/11/18	P078	NA	NA	NA	89	63	131.8	390.0	1113	DI	5.8	6.1
29.....	1997 Nov 6	11:54	12:08	2/1/4	S18W63	X9.4	11:49	11:55	266	360	1607.4	1607.4	6	DU	4464.9	-131.0
30.....	1997 Nov 14	08:30	10:14	3/2/4	N21E70	C4.6	09:05	10:36	79	86	1032.4	800.0	91	DU	146.5	39.6
31.....	1997 Dec 9	11:49	12:55	3/3/2	P225	NA	NA	NA	253	66	332.4	500.0	90	DI	92.6	-12.5
32.....	1997 Dec 14	00:57	02:03	1/1/5	P135	NA	NA	NA	93	72	508.0	600.0	549	DI	18.5	9.5
33.....	1998 Jan 2	23:17	23:28	2/6/7	N22W38	B6.4	23:25	02:25	296	360	397.3	397.3	170	DU	39.0	10.8
34.....	1998 Jan 8	07:56	08:36	1/2/8	S18E60	B3.0	07:20	08:22	69	81	545.5	545.5	62	FL	146.6	1.7
35.....	1998 Jan 25	04:28	10:49	5/7/8	P270	NA	NA	NA	273	75	142.0	200.0	1200	DI	2.8	3.3
36.....	1998 Jan 25	14:29	15:26	3/2/6	N21E25	C1.1	14:29	15:23	112	360	693.0	692.3	54	DU	213.7	-7.4
37.....	1998 Feb 2	17:49	18:27	5/3/4	N25E74	B7.7	17:31	17:55	72	55	501.8	501.8	24	FL	348.5	22.6
38.....	1998 Feb 25	21:44	23:27	3/5/9	NA	NA	NA	NA	74	65	289.0	289.0	150	DI	32.1	1.3
39.....	1998 Mar 22	07:03	07:41	2/5/2	S30E70	M1.1	06:51	07:00	104	49	416.9	416.9	9	FL	772.1	-3.0
40.....	1998 Mar 23	00:01	00:50	7/4/12	P060	NA	NA	NA	94	84	357.8	500.0	49	DI	170.1	-3.0
41.....	1998 Mar 23	07:23	09:33	11/10/ 8	NA	NA	NA	NA	271	111	308.8	400.0	640	DI	10.4	9.2
42.....	1998 Mar 27	00:47	01:23	7/3/6	N30E41	C1.0	00:36	00:46	88	87	568.1	568.1	10	FL	946.9	2.1
43.....	1998 Apr 21	18:04	19:03	3/2/6	P315	NA	NA	NA	292	62	527.0	526.0	126	DI	69.6	6.1
44.....	1998 May 6	23:48	00:02	3/1/4	S16W60	M2.5	23:27	23:46	110	55	784.8	784.8	19	FL	688.4	-9.7
45.....	1998 May 8	01:36	02:28	3/3/6	S16W83	M3.1	01:49	02:04	287	76	371.0	600.0	15	FL	666.7	-0.1
46.....	1998 May 31	03:46	04:26	3/1/4	P120	C2.0	03:53	05:15	88	112	692.2	692.2	82	FL	140.7	8.7
47.....	1998 Jun 2	07:54	08:08	4/2/3	P225	NA	NA	NA	245	57	764.7	1150.0	285	DI	67.3	52.0
48.....	1998 Jun 11	23:28	00:05	15/3/8	P070	C1.1	23:11	00:14	79	58	499.3	499.3	63	DU	132.1	2.8
49.....	1998 Jun 11	09:01	10:28	9/1/6	P070	M1.4	09:57	10:27	123	177	830.1	830.1	30	DU	461.2	-4.9
50.....	1998 Jun 16	18:01	18:27	1/2/4	P240	M1.0	18:03	18:42	341	281	1481.7	1481.7	39	FL	633.2	-74.6

[a] The three subfields show the number of images a CME is seen in LASCO C1, C2, and C3, respectively.

[b] The surface source region location of CMEs, represented by heliographic coordinate if on the front disk, and by position angle if from the limb.

[c] *GOES* X-ray flare magnitude. The next two columns are for the start time and the peak time of flares.

[d] Position angle of CMEs, from NRL/GSFC/CUA CME catalog.

[e] Angular width of CMEs, from NRL/GSFC/CUA CME catalog.

[f] Propagation velocity of CMEs, from NRL/GSFC/CUA CME catalog.

[g] Final velocity of CMEs. They are the same as the propagation velocity for most events, except those of gradual acceleration.

[h] The duration of the main acceleration.

[i] The method used in determining CME main acceleration.DI, FL, and DU indicate the direct method only, indirect flare-proxy method only, and dual methods, respectively.

[j] Magnitude of main acceleration.

[k] Magnitude of residual acceleration, from NRL/GSFC/CUA CME catalog.

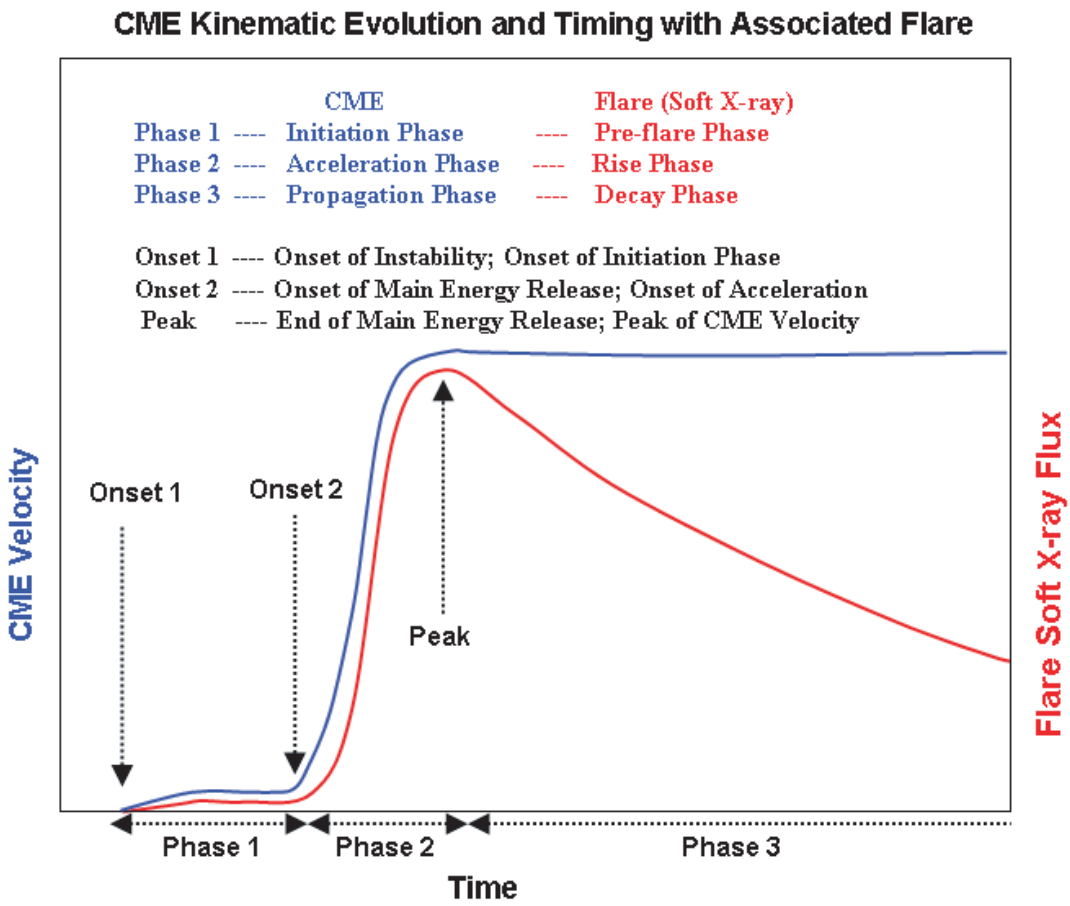

FIG. 1.—Schematic plot of CME kinematic evolution and its relation with temporal evolution of *GOES* soft X-ray flare. CME evolution may have three distinct phases: initiation phase, acceleration phase, and propagation phase, which correspond to the preflare phase, rise phase, and decay phase of the associated flare, respectively.

it emerges above the necessary occulter. The second effect is due to the angular-dependence of the electron Thomson scattering: the scattering is less efficient when an electron is further away from the plane of the sky (Vourlidas et al. 2000)

In Table 1 we list the observed properties of the 50 events selected in the order of observation date. The second and third columns show the first appearance times of CMEs in C1 and C2, respectively. The next column, which has three subitems, shows the number of times a CME was seen in C1, C2, and C3, respectively. Slower events should be seen in more images because it takes the CME a longer time to travel across the fields of view of the coronagraphs than a faster CME. The next column indicates the surface source region locations of CMEs, which are represented by heliographic longitude/latitude coordinates if the source region is on the front side, and by position angle if the source region is not seen on the disk but above the limb. Five events that originated from the backside of the Sun are indicated by NA. The properties of the associated flares (if any) are shown in the next thee columns, which are for *Geostationary Operational Environmental Satellite* (*GOES*) soft X-ray flare magnitude, start time, and peak time, respectively. The following three columns show the CME properties measured in C2 and C3, which are for central position angle, angular width, and velocity (averaged across the C2 and C3 fields of view), respectively (adopted directly from the CDAW CME catalog). The next column shows the CME final velocity at the end of the main acceleration phase. Note that, for many of the 50 events, this velocity is close to the average velocity seen in C2 and C3, and if this is the case, the velocity is directly adopted from the previous column. However, for a number of events, the CME final velocity is very different from the average velocity in C2 and C3, especially for those events for which a significant portion of the main acceleration occurs in the C2 and C3 fields of view, e.g., gradual CME events with long and slow acceleration. The next column shows the duration of the main acceleration phase, which can be derived using two independent methods: a direct method and an indirect flare-proxy method; which method is used is indicated in the next column by "DI" (direct), "FL" (indirect, flare-proxy), or "DU" (dual methods) (see next section for a detailed explanation). The next column shows the magnitude of the main acceleration, which is the result of the CME final velocity divided by the acceleration duration. The residual acceleration of CMEs, which is the average acceleration seen in the C2 and C3 fields of view, is shown in the last column. The value is directly adopted from the CDAW CME catalog.

3. DETERMINING CME ACCELERATIONS AND RELATIONS WITH FLARES

3.1. *Direct Method*

The direct method is to simply interpret the CME velocity profile, directly derived from the measured height-time profile. This method works for those CMEs that have a sufficient number of C1 observations that the main acceleration phase of CME can be separated from the subsequent propagation phase. This normally requires at least three CME images seen in C1. Similar

studies, including several example events and their height-time and velocity-time plots, can be found in our previous works (Zhang et al. 2001, 2004). Instead of repeating the plots here, we summarize the observational properties in the sketch shown in Figure 1. This sketch is largely adopted from the velocity-time plot of the 1998 June 11 event published in Zhang et al. (2001). As indicated in the sketch, the full kinematic evolution of a CME undergoes three distinct phases: (1) an initiation phase, (2) an acceleration phase, and (3) a propagation phase. This scenario of CME kinematic evolution is also consistent with the observations of a much larger number of events investigated in this study. Simply put, phase 1 is characterized by a slow ascension of a large-scale coronal structure (e.g., top envelope of an active region in the corona) for a period up to tens of minutes at a more or less constant speed of a few km s^{-1} to tens of km s^{-1}. Phase 2, or the (main) acceleration phase, is characterized by a period of fast velocity increase, which lasts from a few minutes to tens of minutes (even longer for a few hours for more gradual events). Phase 1 and 2 take place mainly in the inner corona in the C1 field of view. After the acceleration phase, a CME seems fully developed and propagates away with a more or less constant speed, a constant angular width and a constant position angle; hence, we simply call it the propagation phase. The main acceleration we are measuring refers to the rate of velocity change in phase 2, while the residual acceleration refers to that in phase 3.

Because of the nature of the multiple-phased evolution, it is essential to use piecewise fitting methods to derive the velocity and acceleration profiles from the height-time measurement. A piecewise fitting is to find velocity at a local time using two or three adjacent height-time points, equivalent to the first-order numeric derivative. Based on such obtained velocity profiles, we are able to track the velocity change point to point, and identify the onset and ending times, and hence the duration of the CME acceleration phase. The acceleration magnitude is simply the velocity increase during the acceleration phase divided by the acceleration duration. The uncertainty of the acceleration duration is simply determined by the observational cadences, which vary for C1, and are about 30 minutes for C2. For many of the events studied, the uncertainty of acceleration duration is about 30 minutes. The uncertainty of the calculated acceleration magnitude is largely inherited from the uncertainty of the duration. The uncertainty of velocity change should be relatively small, e.g., less than 10%. As a result, the acceleration magnitude uncertainty is small for more gradual events, and large for more impulsive events. In this study, we limit ourselves to applying the direct method for more gradual events, e.g., those having acceleration duration longer than 30 minutes. Therefore, the uncertainty should be less than 50% for these events, and about 15% for those events whose acceleration duration is longer than 100 minutes. For more impulsive events, we use the indirect flare proxy method to determine the CME acceleration, described in the next subsection.

3.2. *Indirect Method and Temporal Relationship Between CMEs and Flares*

If a CME is associated with a *GOES* soft X-ray flare that occurs on the front disk, we are able to use the indirect flare-proxy method to obtain the two acceleration parameters, even if the acceleration is impulsive and there are only one or two CME images seen by C1. This method is based on the assumptions that (1) the rise time of the associated soft X-ray flare equals the CME acceleration time, and (2) the average velocity in the outer corona equals the velocity increase during the acceleration phase.

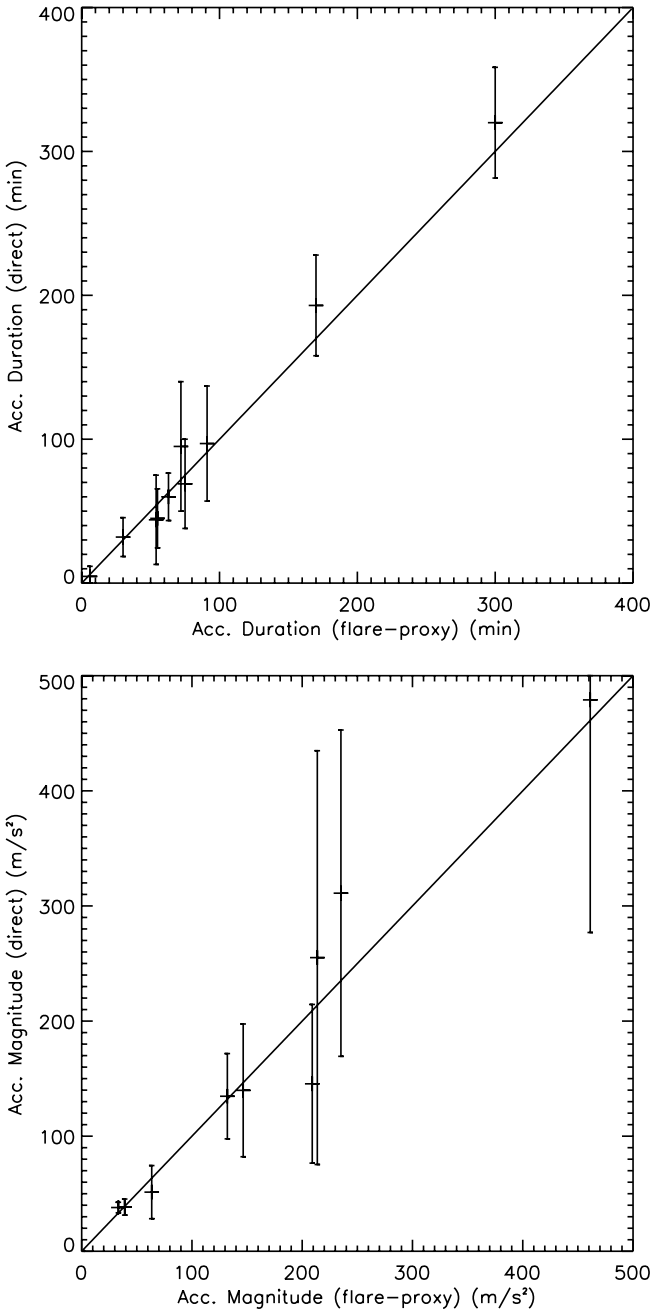

FIG. 2.—Comparison of CME acceleration duration (*top panel*) inferred from the direct method (*Y*-axis) and the indirect flare-proxy method (*X*-axis). The bottom panel shows the comparison of CME acceleration magnitudes. The solid diagonal lines indicate the equal values of the two methods.

These assumptions are justified by the observational fact that the CME acceleration phase usually coincides with the soft X-ray flare's rise phase, which was first demonstrated by Zhang et al. (2001). The sketch in Figure 1 also summarizes the temporal relationship between CME kinematic evolution and flare flux evolution. "Onset1 1" in the figure indicates the start of the slow-rise initiation phase of CME, during which a small enhancement of soft X-ray flux might appear. "Onset 2" indicates the onset time of the main CME acceleration phase, which is also the onset time of the associated flare. The flare start time listed in the NOAA *GOES* flare catalog will correspond to the time at "onset 2," because it marks the fast rise of soft X-ray flux. Further, the main acceleration phase almost ends at the

peak of the soft X-ray flare. This kind of temporal coincidence between flare and CME, or CME-related-ejecta (e.g., filaments), has also been shown by many other studies (Gallagher et al. 2003; Shanmugaraju et al. 2003; Qiu et al. 2004; Maricic et al. 2004; Kundu et al. 2004; Sterling & Moore 2005; Jing et al. 2005)

To further strengthen this point, we studied a subset of 10 events whose accelerations can be determined from both direct and indirect methods; these events are indicated by "DU" in column "TY" in Table 1. Figure 2 shows the comparison of the two accelerations. As shown in the top panel, the data points almost follow the straight diagonal line, indicating that the acceleration duration from the direct method is almost equal to that of the indirect method. The small deviation from the diagonal line is within the error bar, or the uncertainty associated with the direct method. This holds true for all events, ranging from extremely impulsive ones (e.g., event 1997 October 19, a few minutes acceleration) to extremely gradual ones (e.g., event 1996 October 5, 300 minutes of acceleration).

The acceleration magnitudes, shown in the bottom panel, also reveal the closeness of the values inferred from the two methods. Any deviation from the diagonal equal-line is within the error bar. Nevertheless, the uncertainty of acceleration magnitude from the direct method becomes larger for those strongly accelerated events, which are usually impulsive. Note that the extremely impulsive 1997 October 19 event is not plotted in the bottom panel, because its extremely large acceleration values are well beyond the plotting range. For this particular event, the acceleration duration is 6 minutes and the magnitude is 4464.9 m s^{-2} from the indirect method, while the duration is about 4.7 minutes and the magnitude is 7678.6 m s^{-2} from the direct method. This difference is also within the uncertainty associated with the direct method. For impulsive events, the acceleration parameters inferred from indirect method are probably more accurate than that from direct method.

In summary, out of the 50 events studied in this paper, the acceleration of 23 events, which are more gradual, are determined by the direct method only, while 17 events, which are more impulsive, are determined by the indirect flare-proxy method only. The accelerations of the remaining 10 events can be determined by both methods. For these dual events, we use the values determined from the indirect method for subsequent statistical analysis; the acceleration parameters listed in Table 1 are also from the indirect method.

4. RESULTS

4.1. *Distributions of Main and Residual Accelerations*

Figure 3 shows the distribution of the CME (main) acceleration and the residual acceleration for the 50 events studied. The *X*-axis denotes the event number as listed in Table 1. Note that the data point for event numbered 29 (1997 November 6) is omitted from the plot because of its exceptionally high value. The main acceleration spans the whole plotting range along the *Y*-axis, whereas the residual acceleration is limited to a very narrow range clustering around the solid horizontal line indicating zero acceleration. The statistical values about the distributions are listed in Table 2. For the 50 events, the median (average) value of the main acceleration is 170.1 m s^{-2} (330.9 m s^{-2}), while that of the residual acceleration is only 3.1 m s^{-2} (1.0 m s^{-2}). The standard deviation of the main acceleration is as large as 644.8 m s^{-2}, while the standard deviation of the residual acceleration is only 25.3 m s^{-2}. The maximum value of the main acceleration is 4464.9 m s^{-2}, and the minimum value of the main acceleration is 2.8 m s^{-2}. On the other hand, the maximum value for the residual acceleration is 52.0 m s^{-2}, and the maximum negative value, which corresponds to deceleration, is −131 m s^{-2}.

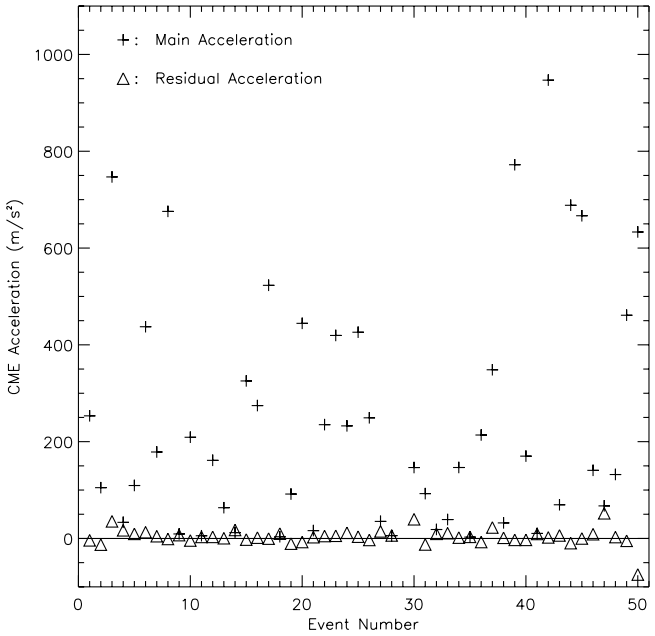

FIG. 3.—Distribution of CME main acceleration (*plus signs*) and residual acceleration (*triangles*) for the 50 events studied. The *X*-axis denotes the event number as listed in Table 1. The solid horizontal line indicates zero acceleration.

In Figure 4 we show the histogram distribution of the same parameters. The extreme event of 1997 November 6 is also omitted from the plots for the sake of showing details for other events. The histogram plots demonstrate again that the main acceleration has a wide range, whereas the residual acceleration is limited to a small range centered around zero. One interesting fact is that the histogram of the main acceleration shows a single major peak at the lower end. The secondary peak at 700 m s^{-2} has only three events and may not be physically significant. Overall, there is no strong signature of a bimodal distribution of the acceleration. This implies that it is not appropriate to divide CME events into simply two classes (see discussion). For the residual acceleration, the distribution is centered around zero value, which is consistent with the view that CMEs display a largely constant speed in the outer corona.

In addition to the magnitude, another important parameter of (main) acceleration is the duration, whose distribution is shown in Figure 5. Like the magnitude, the duration also has a wide distribution, ranging from 6 minutes to about 1200 minutes. The median value is 54 minutes for the 50 events studied. The average value is 180 minutes. The histogram also shows a continuous distribution, with no sign of bimodal distribution. The implication of these observational results on CME classification will be discussed later.

4.2. *A Scaling Law between Magnitude and Duration of Main Acceleration*

One intriguing finding is that there is a strong inverse linear correlation between the acceleration magnitude and the acceleration duration as shown in Figure 6. This correlation is almost identical for the events measured by the direct method (*triangles*) and those events inferred from the indirect flare-proxy method (*plus signs*). This kind of correlation has been reported earlier in a preliminary study based on a smaller sample of events

TABLE 2
STATISTICS OF MAIN AND RESIDUAL ACCELERATIONS

Parameter	Main Accelleration		Residual Acceleration Magnitude ($m\ s^{-2}$)
	Duration (minutes)	Magnitude ($m\ s^{-2}$)	
Median	50.0	170.1	3.1
Average	180.0	330.9	0.9
Standard deviation	285.9	644.8	25.3
Minimum	6.0	2.8	−131.0
Maximum	1200.0	4464.9	52.0

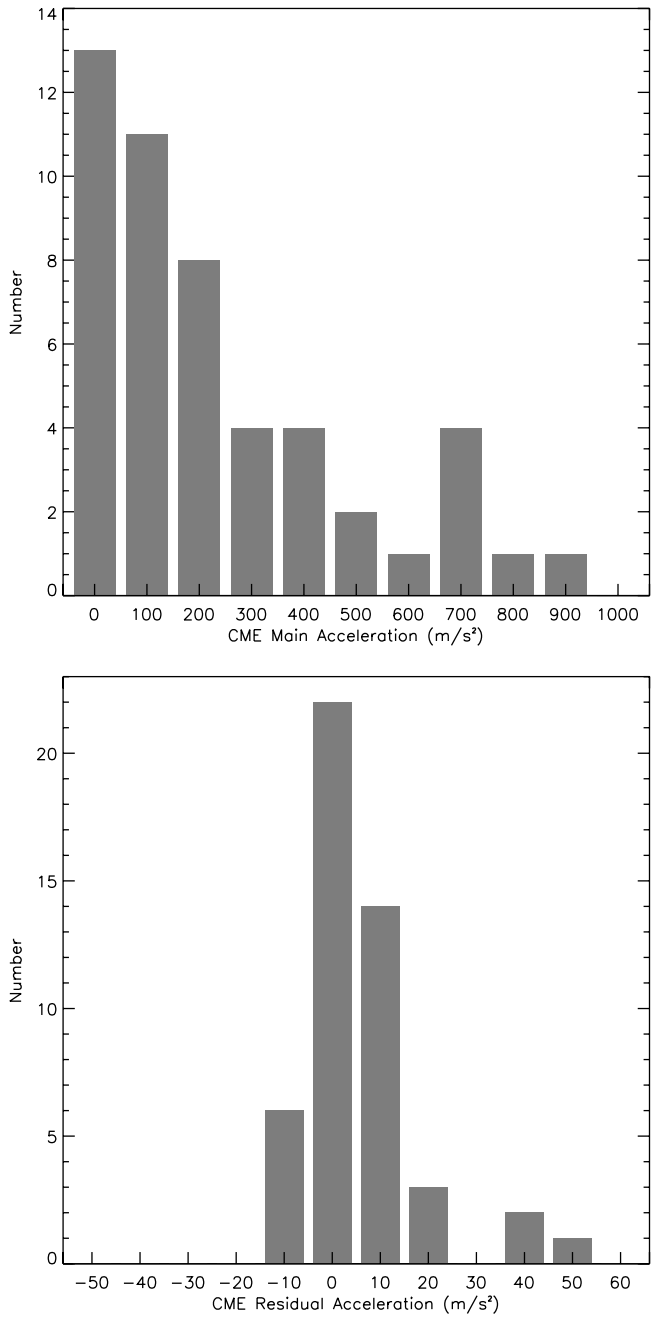

FIG. 4.—Histogram of the main acceleration (*top panel*) and the residual acceleration (*bottom panel*) for the 50 events studied.

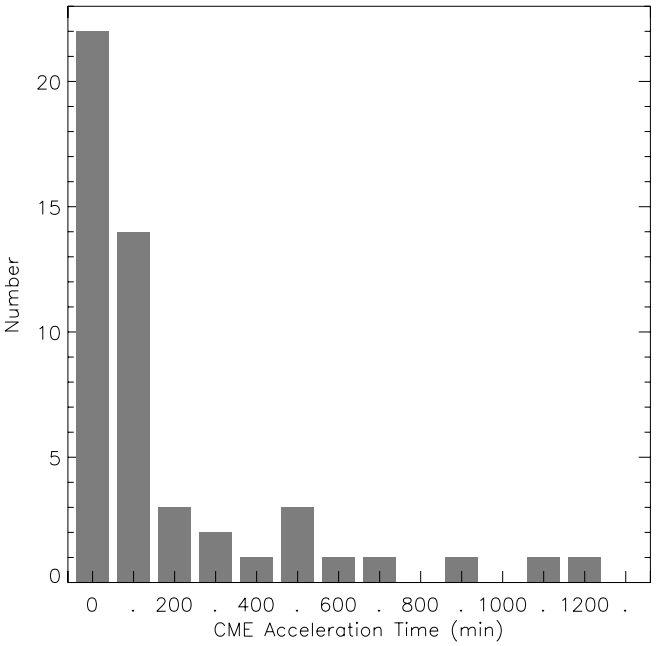

FIG. 5.—Histogram of the acceleration duration during the main acceleration phase for the 50 events studied.

(Zhang 2005). The inverse correlation holds for the whole range of the acceleration parameters, which vary by more than 2 orders of magnitude. The relation can be described by a linear fit,

$$\log(A) = 4.07 - 1.09 \log(T), \quad (1)$$

where A is the acceleration magnitude in unit of $m\ s^{-2}$ and T is the acceleration duration in units of minutes. The correlation coefficient is −0.95, indicating a strong correlation. Considering the uncertainty of measurement, we could round off the

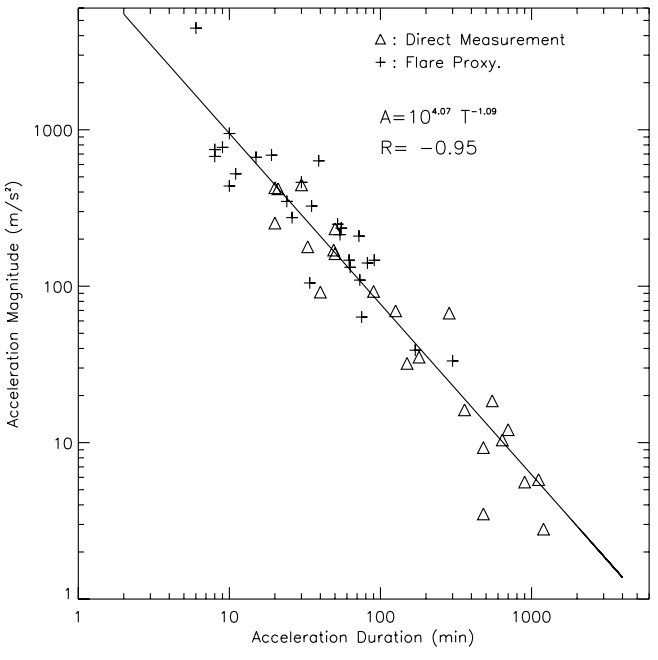

FIG. 6.—Scattering plot of the magnitude vs. the duration of the CME main acceleration phase for the 50 events studied. There is a scaling law between the two acceleration parameters.

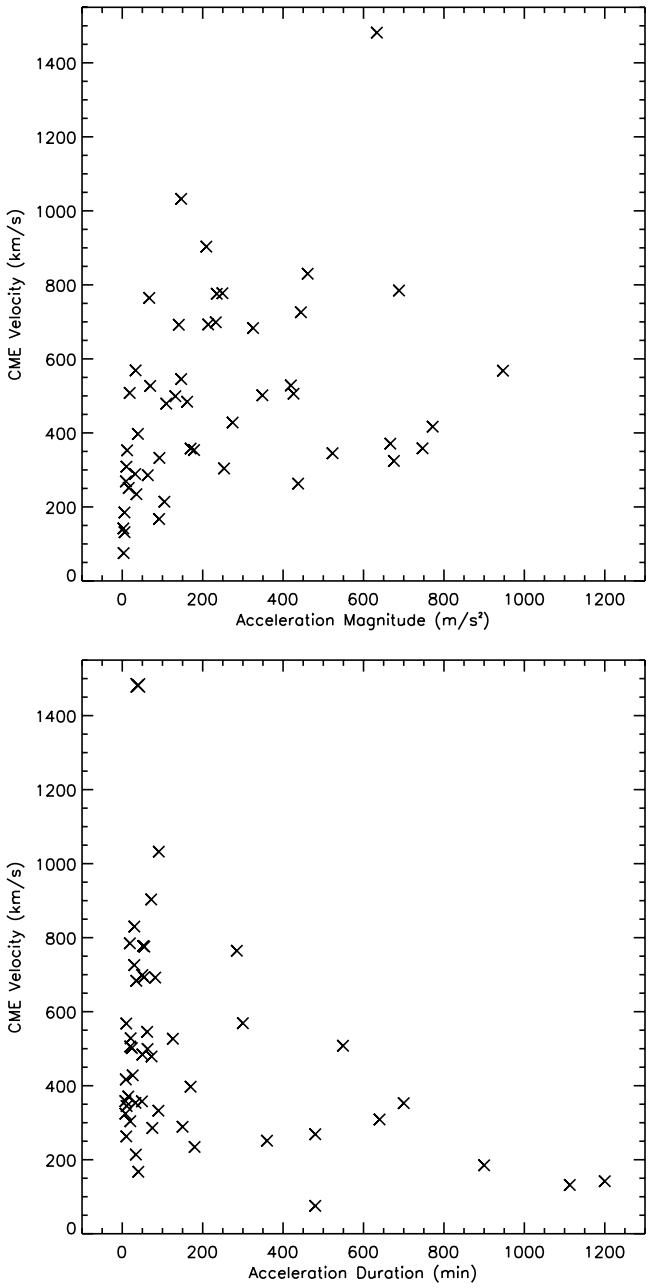

FIG. 7.—Scattering plots of CME velocity vs. acceleration magnitude (*top panel*), and CME velocity vs. acceleration duration (*bottom panel*). There is no apparent correlation between these parameters.

decimal points of the fitted parameters, which yields the simple expression

$$A = 10,000T^{-1}. \quad (2)$$

This formula reveals a scaling law of CME acceleration between the magnitude and the duration. More impulsive events tend to have stronger acceleration, whereas more gradual events tend to have weaker acceleration. When the formula is rewritten as $V = AT = 10,000$ m s^{-2} minutes, or $V = 600$ km s^{-1}, it implies that on average all CME events will have the same final speed of 600 km s^{-1}.

However, a CME's final velocity may vary from a few hundred to about 3000 km s^{-1} from event to event. The final speed of a CME is determined by the combination of two factors: the acceleration magnitude and the acceleration duration; both are important in determining the final speed of a CME. To further clarify this point, we show the scattering plots between CME velocity and acceleration magnitude (Fig. 7, *top panel*), and between CME velocity and acceleration duration (Fig. 7, *bottom panel*). There is no apparent correlation between CME velocity with either acceleration parameter. This implies that neither factor is dominant in determining the final velocity of a CME. It would be interesting to find out what physical mechanism(s) control the acceleration duration and what control the acceleration magnitude. However, this is beyond the scope of this paper.

5. DISCUSSION

5.1. *The Issue of CME Classification*

As shown above, the statistical distributions of CME acceleration, both magnitude and duration, show a continuous behavior. There is no strong sign of a bimodel distribution on acceleration. The earlier study on CME acceleration by St. Cyr et al. (1999) did not show this either. Further, the statistical distribution of CME velocity of thousands of events consistently showed a continuous distribution with a single peak (Howard et al. 1985; Hundhausen et al. 1994; St. Cyr et al. 2000; Yashiro et al. 2004; Yurchyshyn et al. 2005). Therefore, the parameters describing CME kinematic properties, including velocity, acceleration duration and acceleration magnitude, all show a continuous distribution.

In the literature a variety of events have been reported, ranging from extremely impulsive events to extremely gradual ones. St. Cyr et al. (1999) reported the largest acceleration among the 46 events they investigated to be 3270 m s^{-2}. Zhang et al. (2001) reported a CME event with an acceleration as high as 7300 m s^{-2}. Alexander et al. (2002) reported that a CME-associated X-ray ejecta had a peak acceleration of about 4800 m s^{-2}, based on *Yohkoh* SXT observations. Gallagher et al. (2003) found a CME-associated EUV ejection feature reaching a peak acceleration of about 1500 m s^{-2}, based on *Transition Region and Coronal Explore* (*TRACE*) observations. All these extremely impulsive eruptive events are associated with X class flares. MacQueen & Fisher (1983) found that a number of events had fast but constant speed beyond a projected height of 0.2 $R_\odot$ above the limb; these events must also be very impulsive because the acceleration took place within a very short distance. On the other hand, there are CMEs characterized by a very weak acceleration ($<$20 m s^{-2}) over a long duration (several hours) and a long distance (e.g., up to 15 $R_\odot$) (Sheeley 1999; Sheeley et al. 1999; Srivastava et al. 1999, 2000). These are extremely gradual CMEs. They do not show a phase of fast acceleration. These CMEs are often not associated with any flares.

Nevertheless, most CME events reside between the extremely impulsive ones and the extremely gradual ones, characterized by acceleration in the order of hundreds of m s^{-2}. Jing et al. (2005) found that the accelerations of erupting filaments are mainly in the range of 50–400 m s^{-2}. Individual events with normal accelerations have been reported by many studies (Wood et al. 1999; Shanmugaraju et al. 2003; Qiu et al. 2004; Vršnak et al. 2004; Kundu et al. 2004; Sterling & Moore 2005). Zhang et al. (2004) showed an event (2000 October 25) with an acceleration duration of about 160 minutes and a magnitude of about 131 m s^{-2}. This moderate acceleration continued until the CME reached a height of about 7.0 $R_\odot$. Events with similar intermediate kinematic characteristics have been reported before (Plunkett et al. 2000; Yurchyshyn 2002).

The continuous distribution of CME kinematic properties is not consistent with the speculation that there may be two distinct classes of CMEs: impulsive CMEs and gradual CMEs (Sheeley et al. 1999; Andrews & Howard 2001; Moon et al. 2002; Zhang et al. 2002). These studies are based on a small number of selected events or selective events. Statistical analysis by Yurchyshyn et al. (2005) showed that the speed distribution for accelerating and decelerating events in the LASCO C2 and C3 fields of view are nearly identical and to a good approximation they can be fitting with a single lognormal distribution. Vršnak et al. (2005) found that flare-associated CMEs and nonflare CMEs showed quite similar characteristics in the LASCO C2 and C3 fields of view, contradicting the concept of two types. We believe that the usage of the impulsive and gradual types should be limited to the convenience of reference. They should not be regarded as specific classes that are physically distinct from other events, since they are part of a continuous distribution.

5.2. *Implications on CME Modelings*

Here we discuss the implications of our observational results, along with other relevant observations, on CME modelings. We consider the following three observational facts: (1) the wide and continuous distribution of CME acceleration in both magnitude and duration, and the scaling law of the acceleration; (2) the close temporal coupling between the CME bulk acceleration that occurs in macro scale and the flare particle acceleration that occurs in micro scale; and (3) the multiple-phase kinematic evolution of CMEs. A successful theoretical model should be able to explain these observational facts, regardless of its initial magnetic configuration, trigger process, and subsequent dynamic evolutions.

The temporal coincidence between CME acceleration and flare flux increase suggests that the run-away process of CME eruption is strongly coupled with the magnetic reconnection process that causes the flare. It has been widely accepted that a flare is caused by the magnetic reconnection process, which rapidly dissipates the magnetic energy prestored in the corona. Nonthermal energetic particles are accelerated inside or in the vicinity of the reconnection region through various possible mechanisms (e.g., see review by Priest & Forbes 2002). When these energetic particles precipitate from the corona into the chromosphere along magnetic field lines, they spontaneously produce the hard X-ray emissions through the bremsstrahlungmechanism, and subsequently in an accumulation manner produce the soft X-ray emissions from the heated plasma evaporated from the chromospheric layer into the corona (e.g., Li et al. 1993). The evaporation process results in the well known "Neupert" effect between the soft X-ray profile and the hard X-ray profile of a flare: the time-derivative of the soft X-ray profile resembles the corresponding hard X-ray profile, especially during the soft X-ray flare's rise phase (Neupert 1968; Dennis & Zarro 1993). Therefore, the rise phase of soft X-ray flare is believed to correspond to the main energy release phase in the corona through the magnetic reconnection. Further, it is found that, using filament eruption as a proxy, main CME acceleration occurs during the period of fast flare ribbon separation, a known signature of magnetic reconnection in the corona (Qiu et al. 2004; Jing et al. 2005). Qiu & Yurchyshyn (2005) recently showed a good correlation between the reconnected magnetic flux and the final speed of CMEs. These observations suggest that the reconnection play an active role in CME acceleration. It is consistent with the traditional eruptive flare models, in which the driver is the magnetic reconnection underneath the rising prominence (Hirayama 1974; Kopp & Pneuman 1976). The basic idea of the eruptive flare models is adopted by many CMEs models, in which the magnetic reconnection occurs in the current sheet produced by the stretching of the erupting magnetic field, leading to the impulsive release of magnetic energy and the fast ejection of magnetic flux rope (Mikic & Linker 1994; Lin & Forbes 2000; Amari et al. 2000; Chen & Shibata 2000; Moore et al. 2001; Cheng et al. 2003). In these models, the reconnection plays a role of fast tether-cutting, which effectively disconnect the magnetic field lines from their foot points tied with the photosphere. In addition to the reconnection underneath the flux rope, the CME break-out models (Antiochos et al. 1999; MacNeice et al. 2004) also involve the magnetic reconnection above the escaping flux rope in a multipolar magnetic configuration.

The temporal coincidence also suggests that the CME run-away process and the magnetic reconnection process may mutually feed each other. The two processes not only start at the same time, but also end at almost the same time based on observations. The magnetic tether-cutting process is known to be very effective in accelerating the CME flux rope (Vršnak et al. 2004). First, it reduces the tension of the overlying restraining field by cutting the tie with the photosphere. Second, it increases the magnetic pressure below the flux rope by adding the poloidal flux through reconnection. Third, it enhances the outward hoop force due to the curvature of the flux rope thanks to the poloidal flux added. The escape of the flux rope reduces the magnetic pressure below, and thus induces an inflow toward the central current sheet; the current sheet is caused by the magnetic stretch as a result of the rising flux rope. Therefore, a faster rise of the flux rope causes a faster inflow, which results in a faster tether-cutting reconnection. At the same time, a faster reconnection causes a stronger outward force and thus a faster CME acceleration. The whole process, through flux rope rising, magnetic field stretching underneath, inflow tether-cutting reconnection, and further accelerating, forms a closed loop of positive feeding, which leads to the simultaneous CME acceleration and flare energy release.

Another fact is that a CME may undergo multiple phases of kinematic evolution. Before the onset of the main acceleration (and also the onset of the flare), it is often observed that a CME (or a filament) undergoes a slow-rise phase (Kahler et al. 1988; Zhang et al. 2001; Maricic et al. 2004; Kundu et al. 2004; Schuck et al. 2004; Sterling & Moore 2005), This phase is not trivial, because its rising speed is about 10–100 km s^{-1} and it may last for tens of minutes. This phase is certainly different from the nominal energy built-up phase driven by the photospheric movements, which, including the shearing motion, flux-cancellation, and flux-emergence, are all in the order of a few km s^{-1}, too small to account for the rising velocity. The magnitude of the rising velocity in the initiation phase indicates that the involved magnetic structure, possibly flux rope, has lost the quasi-static equilibrium. On the other hand, because of the lack of strong X-ray emission, there is no fast magnetic reconnection in this phase. The loss of the mechanic equilibrium has long been considered to be the trigger of the subsequent main energy release (Hirayama 1974). It is likely that the rising motion leads to the formation of the current sheet underneath, and the continuing rising motion stretches and strengthens the current sheet and eventually reaches the critical point that the fast magnetic reconnection sets in. Once the reconnection is triggered, the positive mutual feeding processes described above cause the rapid energy release and the eruption of the involved magnetic structure. Most computational CME models introduce a continuous shearing motion of the magnetic field in the photosphere to build up the free energy in the corona and drive the eruption of the system. These models usually show a transition from slow to fast motion of the erupting magnetic structure (Mikic & Linker 1994; Lin & Forbes 2000; Chen & Shibata

2000; MacNeice et al. 2004). But, the transition in the models seems to be smooth, It is desirable to have models to demonstrate the distinct phases of CME kinematic evolution and review the transition mechanisms from phase to phase. There are at least four phases that a model should address: (1) the very slow energy build-up phase driven by the photospheric motion in the order of 1 km s^{-1}, (2) a slow rise phase of certain erupting feature on the order of 10 km s^{-1}, (3) a fast acceleration phase in the order of 100 km s^{-1}, and (4) the near constant-speed propagation phase.

Finally, a robust theoretical model should explain the wide distribution of the kinematic properties of CMEs, including the distributions of the acceleration (from $\sim$10 to $\sim$5000 m s^{-2}, from $\sim$5 to $\sim$1000 minutes), the velocity (from $\sim$50 to $\sim$3000 km s^{-1}), and the size (from $\sim 10^{\circ}$ to $\sim 180^{\circ}$). Further, a good model should also explain the observed scaling law between the magnitude of the acceleration and the duration of the acceleration.

6. CONCLUSIONS

We have made a statistical study of the main and residual accelerations of CMEs. This is probably the first statistical study of the CME main acceleration in the inner corona. The obtained parameters shall enrich those parameters obtained before, including mass, size, velocity, and residual acceleration. We found that the two accelerations are indeed distinctly different. For the 50 events studied, the magnitude of the main acceleration ranges from 2.8 to 4464.0 m s^{-2}, with a median (average) value of 170.1 (330.9 m s^{-2}) and a standard deviation of 644.8 m s^{-2}, whereas the magnitude of the residual acceleration ranges only from -131.0 to 52.0 m s^{-2} with a median (average) value of 3.1 (0.9 m s^{-2}) and a standard deviation of only 25.3 m s^{-2}. This result reinforces the view that there are distinct evolution phases of CMEs. We have further demonstrated that CME acceleration phase coincides with flare flux rise phase. Indeed, we have exploited this fact and infer the CME acceleration duration using the rise time of associated flare. This indirect method is particularly useful for more impulsive events for which a direct measurement of acceleration is not possible. The duration of the main acceleration ranges from 6 to 1200 minutes, with a median (average) value of 54 (180 minutes) and a standard deviation of 286 minutes.

The CME main accelerations, in terms of both magnitude and duration, have a wide distribution that spans over almost 3 orders of magnitude. This wide distribution represents a continuous spectrum of CMEs events, ranging from extremely gradual ones all the way to the extremely impulsive ones. The histogram of CME accelerations shows a smooth profile with a single peak. The lack of bimodal distribution implies that it is not appropriate to classify CMEs into two simple classes, impulsive or gradual. We also find that the final velocity of a CME should be determined by the two acceleration factors: magnitude and duration. Neither factor is dominant in determining a CME's final speed. Finally, we find an interesting scaling law between the acceleration magnitude (A) and the acceleration duration (T) over the entire parameter range: $A(\mathrm{m\ s^{-2}}) = 10,000T^{-1}$ (minutes). In logarithmic scale, the linear correlation coefficient is as high as 0.95.

J. Zhang is supported by NASA grants NNG04GN36G and NNG05GG19G, and NSF SHINE grant ATM-0454612. *SOHO* is a project of international cooperation between ESA and NASA. The LASCO instrument was constructed by a consortium of the Naval Research Laboratory, University of Birmingham (England), the Max-Planck-Institute für Aeronomie (Germany), and the Laboratoire d'Astronomie Spatiale (France). We acknowledge the usage of the CME catalog generated and maintained at the CDAW Data Center by NASA and The Catholic University of America in cooperation with the Naval Research Laboratory.

REFERENCES

Alexander, D., Metcalf, T. R., & Nitta, N. V. 2002, Geophys. Res. Lett., 29, 41
Amari, T., Luciani, J. F., Mikic, Z., & Linker, J. 2000, ApJ, 529, L49
Andrews, M. D., & Howard, R. S. 2001, Space Sci. Rev., 95, 147
Antiochos, S. K., DeVore, C. R., & Klimchuk, J. A. 1999, ApJ, 510, 485
Brueckner, G. E., et al. 1995, Sol. Phys., 162, 357
Chen, J., & Krall, J. 2003, J. Geophys. Res., 108, 1410
Chen, P. F., & Shibata, K. 2000, ApJ, 545, 524
Cheng, C. Z., Ren, Y., Choe, G. S., & Moon, Y.-J. 2003, ApJ, 596, 1341
Delaboudinière, J.-P., et al. 1995, Sol. Phys., 162, 291
Dennis, B. R., & Zarro, D. M. 1993, Sol. Phys., 146, 177
Gallagher, P. T., Lawrence, G. R., & Dennis, B. R. 2003, ApJ, 588, L53
Hirayama, T. 1974, Sol. Phys., 34, 323
Howard, R. A., Sheeley, N. R., Jr., Michels, D. J., & Koomen, M. J. 1985, J. Geophys. Res., 90, 8173
Hundhausen, A. J., Burkepile, J. T., & St. Cyr, O. C. 1994, J. Geophys. Res., 99, 6543
Jing, J., Qiu, J., Lin, J., Qu, M., Xu, Y., & Wang, H. 2005, ApJ, 620, 1085, 1091
Kahler, S. W., Moore, R. L., Kane, S. R., & Zirin, H. 1988, ApJ, 328, 824
Kopp, R. A., & Pneuman, G. W. 1976, Sol. Phys., 50, 85
Kundu, M. R., White, S. M., Garaimov, V. I., Manoharan, P. K., Subramanian, P., Ananthakrishnan, S., & Janardhan, P. 2004, ApJ, 607, 530
Li, P., Emslie, A. G., & Mariska, J. T. 1993, ApJ, 417, 313
Lin, J., & Forbes, T. G. 2000, J. Geophys. Res., 105, 2375
MacNeice, P., Antiochos, S. K., Phillips, A., Spicer, D. S., DeVore, C. R., & Olson, K. 2004, ApJ, 614, 1028
MacQueen, R. M., & Fisher, R. R. 1983, Sol. Phys., 89, 89
Maricic, D., Vršnak, B., Stanger, A. L., & Veronig, A. 2004, Sol. Phys., 225, 337
Mikic, Z., & Linker, J. A. 1994, ApJ, 430, 898
Moon, Y.-J., Choe, G. S., Wang, H., Park, Y. D., Gopalswamy, N., Yang, G., & Yashiro, S. 2002, ApJ, 581, 694
Moore, R., Sterling, A. C., Hudson, H. S., & Lemen, J. 2001, ApJ, 552, 833
Neupert, W. M. 1968, ApJ, 53, L59
Plunkett, S. P., et al. 2000, Sol. Phys., 194, 371
Priest, E. R., & Forbes, T. G. 2002, A&A Rev., 10, 313
Qiu, J., Wang, H., Cheng, C. Z., & Gary, D. E. 2004, ApJ, 604, 900
Qiu, J., & Yurchyshyn, V. B. 2005, ApJ, 634, L121
Schuck, P. W., Chen, J., Schwartz, I. B., & Yuchyshyn, V. 2004, ApJ, 610, L133
Shanmugaraju, A., Moon, Y.-J., Dryer, M., & Umapathy, S. 2003, Sol. Phys., 215, 185
Sheeley, N. R., Jr. 1999, in AIP Conf. Proc. 471, Solar Wind Nine, ed., S. R. Habbal, R. Esser, J. V. Hollweg and, P. A. Isenberg (New York: AIP), 41
Sheeley, N. R., Jr., Walters, H., Wang, Y.-M., & Howard, R. A. 1999, J. Geophys. Res., 104, 24739
St. Cyr, O. C., Burkepile, J. T., Hundhausen, A. J., & Lecinski, A. R. 1999, J. Geophys. Res., 104, 12493
St. Cyr, O. C., et al. 2000, J. Geophys. Res., 105, 18169
Sterling, A. C., & Moore, R. L. 2005, ApJ, 630, 1148
Srivastava, N., Schwenn, R., Inhester, B., Martin, S. F., & Hanaoka, Y. 2000, ApJ, 534, 468
Srivastava, N., Schwenn, R., Inhester, B., Stenborg, G., & Podlipnik, B. 1999, Space Sci. Rev., 87, 303
Vourlidas, A., Subramanian, P., Dere, K. P., & Howard, R. A. 2000, ApJ, 534, 456
Vršnak, B., Maricic, D., Stanger, A. L., & Veronig, A. 2004, Sol. Phys., 225, 355
Vršnak, B., Sudar, D., & Ruzdjak, D. 2005, A&A, 435, 1149
Wood, B. E., Karovska, M., Chen, J., Brueckner, G. E., Cook, J. W., & Howard, R. A. 1999, ApJ, 512, 484
Yashiro, S., Gopalswamy, N., Michalek, G., St. Cyr, O. C., Plunkett, S. P., Rich, N. B., & Howard, R. A. 2004, J. Geophys. Res., 109, 07105
Yurchyshyn, V. B. 2002, ApJ, 576, 493
Yurchyshyn, V., Yashiro, S., Abramenko, V., Wang, H., & Gopalswamy, N. 2005, ApJ, 619, 599
Zhang, J., Dere, K. P., Howard, R. A., Kundu, M. R., & White, S. M. 2001, ApJ, 559, 452
Zhang, J. 2005, in IAU Symp. 226, Coronal and Stellar Mass Ejection, ed. K. Dere, J. Wang, & Y. Yan (Cambridge: Cambridge Univ. Press), 65
Zhang, J., Dere, K. P., Howard, R. A., & Vourlidas, A. 2004, ApJ, 604, 420
Zhang, M., Golub, L., Deluca, E., & Burkepile, J. 2002, ApJ, 574, L97